ACS Photonics

Article

Cite This: ACS Photonics 2019, 6, 2577−2582

pubs.acs.org/journal/apchd5

Stimulated Emission Depletion Microscopy with Diamond Silicon Vacancy Centers

Yaser Silani,[§] Forrest Hubert,[§] and Victor M. Acosta*

Center for High Technology Materials and Department of Physics and Astronomy, University of New Mexico, Albuquerque, New Mexico 87106, United States

Supporting Information

ABSTRACT: The spatial resolution and fluorescence signal amplitude in stimulated emission depletion (STED) microscopy is limited by the photostability of available fluorophores. Here, we show that negatively charged silicon vacancy (SiV) centers in diamond are promising fluorophores for STED microscopy, owing to their photostable, near-infrared emission and favorable photophysical properties. A home-built pulsed STED microscope was used to image shallow implanted SiV centers in bulk diamond at room temperature. The SiV stimulated emission cross section for 765−800 nm light is found to be $(4.0 \pm 0.3) \times 10^{-17}$ cm^2, which is approximately 2−4 times larger than that of the negatively charged diamond nitrogen vacancy center and approaches that of commonly used organic dye molecules. We performed STED microscopy on isolated SiV centers and observed a lateral full-width-at-half-maximum spot size of 89 ± 2 nm, limited by the low available STED laser pulse energy (0.4 nJ). For a pulse energy of 5 nJ, the resolution is expected to be ∼20 nm. We show that the present microscope can resolve SiV centers separated by ≲150 nm that cannot be resolved by confocal microscopy.

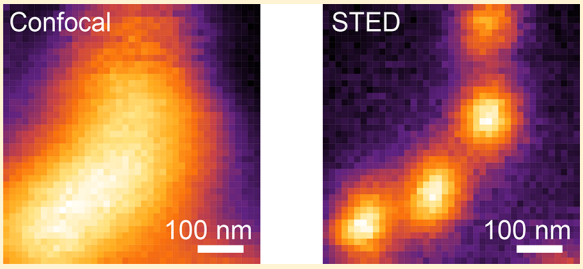

KEYWORDS: *super-resolution, diamond, microscopy, STED, SiV, NV*

Stimulated emission depletion (STED) microscopy is one of several techniques that can image fluorescent molecules with a spatial resolution superior to the optical diffraction limit.[1,2] While the resolution in STED microscopy can theoretically approach the scale of individual atoms,[3] resolving structures at the few nanometer scale in biological samples remains an experimental challenge. This is partly due to a lack of fluorescent probes that possess the requisite photophysical properties and are sufficiently small, bright, photostable, and nontoxic.

In STED microscopy, the theoretical lateral resolution, Δd, scales approximately as $\Delta d \propto \sqrt{I_{sat}/I}$, where I is the optical intensity used to stimulate emission and I_{sat} is the fluorophore's stimulated-emission saturation intensity.[4] This scaling has two consequences for probe design. The first is that a low I_{sat} is desirable so that low enough values of I can be used to avoid sample photodamage while maintaining high resolution. The second consequence is that a high degree of photostability is required to simultaneously realize low values of Δd and a high fluorescence signal amplitude. This is because, when I_{sat}/I is small (as needed for high resolution), many fluorophore absorption events do not produce detectable fluorescence, yet they often have the same propensity for photobleaching.[5] Thus, if the fluorophore bleaches after a fixed number of absorption events, there is an unavoidable trade-off between spatial resolution and fluorescence signal amplitude. A similar argument holds in pulsed STED microscopy, where the STED beam's pulse fluence is substituted for intensity.

Organic dye molecules are among the most widely used fluorophores in STED microscopy.[6] They can be functionalized to specifically bind to biological targets[7] and are relatively nontoxic.[8] They also can produce high fluorescence rates[9] and feature sufficiently low values of I_{sat}[10] to enable imaging of cells with a spatial resolution down to ∼20 nm.[11] Nevertheless, standard organic fluorophores suffer from photobleaching due to irreversible chemical reactions,[12] thereby limiting the achievable fluorescence signal amplitude and resolution.[13]

Solid-state color centers are an intriguing alternative probe for STED microscopy, as the host crystal prevents some forms of photobleaching.[14] For example, the negatively charged nitrogen vacancy (NV) color center in diamond exhibits nearly perfect photostability in nanodiamonds with characteristic dimensions down to ∼10 nm.[15] Moreover diamond is a relatively nontoxic host crystal that can be functionalized to bind to intracellular targets.[16] NV centers in bulk diamond have been used to set record spatial resolutions in STED microscopy, with lateral resolutions as small as Δd = 2.4 nm.[17] However, NV centers have some limitations in their use in STED microscopy. The fluorescence intensity of a single NV center is more than an order of magnitude weaker than a typical organic fluorophore[18] under similar conditions. They require high stimulated emission depletion intensities, owing

Received: August 7, 2019
Published: September 9, 2019

DOI: 10.1021/acsphotonics.9b01135
ACS Photonics 2019, 6, 2577−2582

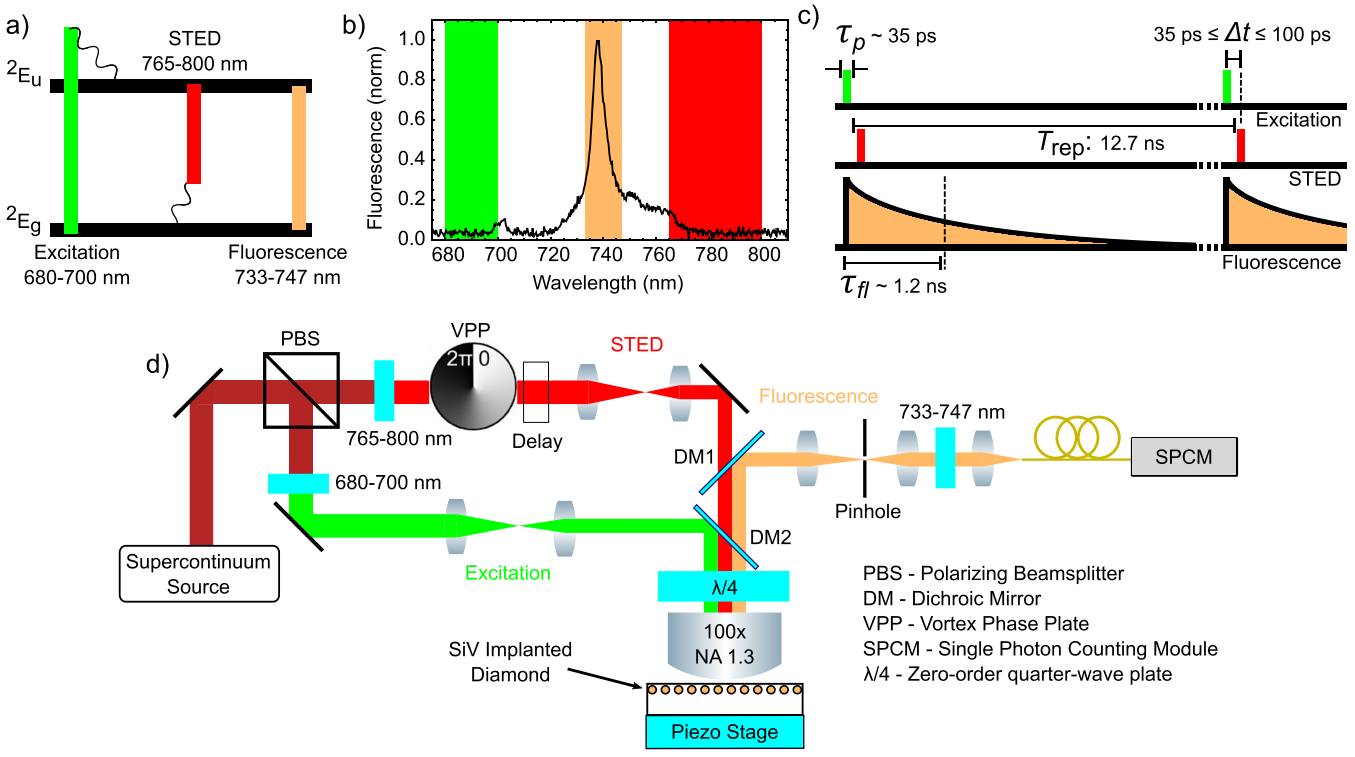

Figure 1. SiV STED methodology. (a) SiV optical transitions between the ground (^2E_g) and excited (^2E_u) electronic states.[24,25] (b) SiV fluorescence spectrum under 685 nm excitation. The bands used for excitation, fluorescence collection, and STED are labeled in green, orange, and red, respectively. The wavelength band of the STED beam (765−800 nm) was selected to maximize the available power from the supercontinuum source, while minimizing anti-Stokes excitation (Section SVII) and remaining within the tail of the phonon sideband. (c) Pulse sequence used for STED microscopy and for measuring the SiV stimulated emission cross section. The pulses are provided by a picosecond supercontinuum source with a repetition rate of 78 MHz. (d) Apparatus used for STED microscopy of SiV centers. An oil-immersion microscope objective with numerical aperture NA = 1.3 focuses light onto, and collects fluorescence from, SiV centers. Additional details are found in the Supporting Information.

to their relatively low cross section (approximately (1−2) × 10^{-17} cm[2][19,20]) and their propensity for excited state absorption.[21,22] Finally, NV centers tend to blink in small nanodiamonds and do not produce observable fluorescence in nanodiamonds smaller than ∼10 nm.[15,23]

Negatively charged silicon vacancy (SiV) color centers in diamond may offer a more promising alternative for STED microscopy applications. SiV centers have been shown to be photostable in nanodiamonds as small as ∼2 nm,[26] and their fluorescence spectrum lies in a narrow band in the near-infrared.[27] Here, we report measurements of the stimulated emission cross section of SiV centers in bulk diamond. We find $\sigma_{STED} = (4.0 \pm 0.3) \times 10^{-17}$ cm^2 for 765−800 nm light. This is approximately 2−4 times larger than the σ_{STED} reported for NV centers and nearly as large as that of organic fluorophores commonly used in STED microscopy.[28,29] We demonstrate STED microscopy on isolated SiV centers in diamond, realizing a resolution $\Delta d = 89 \pm 2$ nm, limited by the available STED laser pulse energy (0.4 nJ). If these properties are similar in sub-10 nm nanodiamonds, and higher STED pulse energies are available, SiV centers may be ideal probes for high-resolution STED microscopy in biological systems. Our methods can also be applied to resolving nanoscale SiV center arrays in quantum information applications.[30,31]

EXPERIMENTAL SETUP

The SiV optical transitions and emission spectrum are shown in Figure 1a and b, respectively. The pulse sequence used for STED microscopy is shown in Figure 1c. A laser pulse (680−700 nm) excites SiV centers on their absorption phonon sideband. A second pulse (765−800 nm), with a time delay of 35 ps $\lesssim \Delta t \lesssim$ 100 ps (Section SIV), stimulates SiV emission on the emission phonon sideband. Fluorescence is collected about the SiV zero-phonon line (ZPL) in the band at 733−747 nm. Both excitation and stimulated emission pulses have a temporal full-width-at-half-maximum (fwhm), $\tau_p \approx 35$ ps (Section SIV), that is considerably shorter than the SiV excited state lifetime ($\tau_{fl} \approx 1.2$ ns[27]). The sequence is repeated after the laser repetition time, $T_{rep} = 12.7$ ns $\gg \tau_{fl}$, which is long enough to ensure SiV centers are initialized in their ground state at the start of each sequence. A schematic of our SiV STED microscope is shown in Figure 1d. A supercontinuum source is used to generate both excitation and stimulated emission pulses. The SiV centers studied here were formed from ion implantation and annealing. They were typically ∼50 nm below the diamond surface with an approximate areal density of 10^6−10^8 cm^{-2}. Section SII contains additional details on the samples and how they were prepared.

RESULTS

Figure 2a displays a confocal image of ZPL emission (733−747 nm) from an isolated SiV center under 680−700 nm excitation. The fwhm of the feature is ∼270 nm, consistent with the diffraction limit of our microscope. Such isolated features were assumed to be single SiV centers based on their sparsity and nearly identical intensity, Section SVI. Figure 2b shows the detected fluorescence intensity of three SiV centers as a function of average excitation power, P_{ex}. We fit these data

DOI: 10.1021/acsphotonics.9b01135
ACS Photonics 2019, 6, 2577−2582

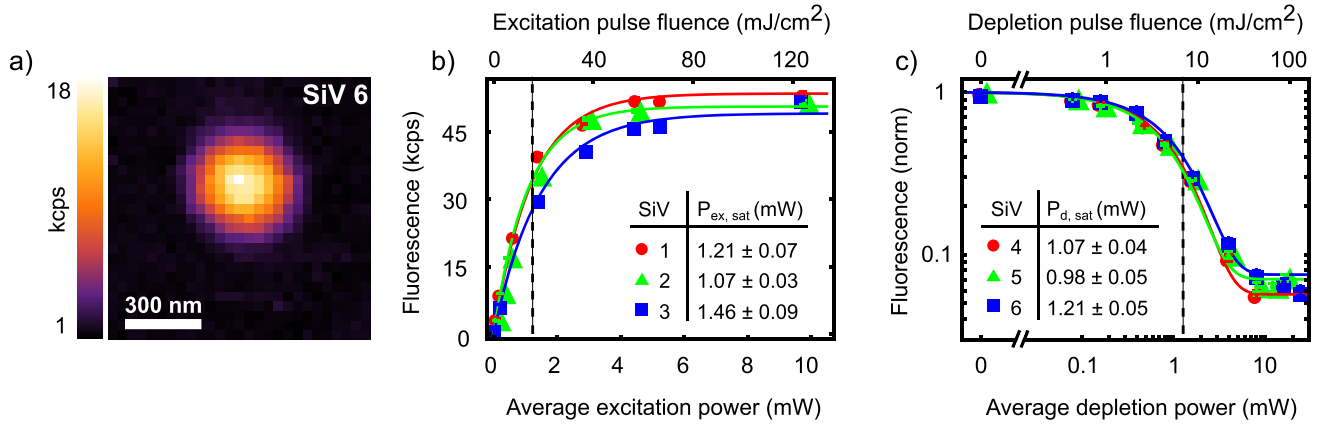

Figure 2. Excitation and depletion saturation curves. (a) Confocal image of ZPL emission (733−747 nm) from an isolated SiV center excited with 680−700 nm light. (b) Fluorescence intensity as a function of average excitation power (or corresponding peak pulse fluence) for three SiV centers. Inset: Table reporting fitted average excitation saturation powers and fit uncertainties for each SiV center. The mean value is annotated as a dashed line on the plot. (c) Normalized fluorescence intensity as a function of average depletion power (or corresponding peak pulse fluence) for three different SiV centers excited at $P_{ex} \approx P_{ex,sat}$. Inset: Table reporting fitted average depletion saturation powers and fit uncertainties for each SiV center. The mean value is annotated as a dashed line on the plot.

to a saturation curve of the form $C = C_{max}(1 - e^{-P_{ex}/P_{ex,sat}})$,[32] where C_{max} is the peak detected fluorescence intensity [typically 45 to 55 kilocounts/second (kcps) for SiV centers in our setup] and $P_{ex,sat}$ is the average excitation saturation power. From the fits, we extract $P_{ex,sat} = 1.2 \pm 0.2$ mW, corresponding to the mean and standard deviation for the set of three SiV centers. By incorporating the laser repetition rate and independently measured intensity profile of the excitation spot (Section SIII), this value converts to a saturation pulse fluence $F_{ex,sat} = 15 \pm 3$ mJ/cm^2. The excitation cross section for this wavelength band is then calculated (Section SIII) as $\sigma_{ex} = E_{ph,ex}/F_{ex,sat} = (1.8 \pm 0.3) \times 10^{-17}$ cm^2, where $E_{ph,ex} = 2.9 \times 10^{-19}$ J is the excitation photon energy. All remaining experiments were performed with average excitation power $P_{ex} \lesssim P_{ex,sat}$.

We determined the stimulated emission cross section for 765−800 nm light, σ_{STED}, using the pulse sequence in Figure 1c with overlapped Gaussian spatial profiles for excitation and depletion beams. Figure 2c shows the normalized fluorescence intensity from three SiV centers as a function of average depletion power, P_d. These data were fit to an exponential decay function, $C \propto e^{-P_d/P_{d,sat}}$, revealing an average depletion saturation power $P_{d,sat} = 1.1 \pm 0.1$ mW (mean and standard deviation for the three SiV centers). This power corresponds to a depletion saturation pulse fluence $F_{d,sat} = 6.8 \pm 0.6$ mJ/cm^2 (Section SIII). The stimulated emission cross section is therefore $\sigma_{STED} = E_{ph,d}/F_{d,sat} = (4.0 \pm 0.3) \times 10^{-17}$ cm^2 (Section SIII), where $E_{ph,d} = 2.5 \times 10^{-19}$ J is the depletion photon energy. This cross section is approximately 2−4 times larger than that of the diamond NV center[19,20] and approaches that of the organic dye molecules, $(3-15) \times 10^{-17}$ cm^2,[28,29] commonly used in STED microscopy.

We next show that STED microscopy applied to SiV centers can be used to realize resolution beyond the optical diffraction limit. We continue to use the pulse sequence in Figure 1c, but now a vortex phase plate is inserted in the STED path to shape its spatial profile into a donut. We recorded STED images of isolated SiV centers at varying donut powers, P_{donut}. Each image is fit to a two-dimensional Gaussian profile to extract the SiV lateral fwhm (Section SV). At least three images were acquired for each SiV center at each power to determine statistical uncertainty. The results are plotted in Figure 3a. Example images taken at $P_{donut} = 0$ and $P_{donut} = 32$ mW (0.4 nJ pulse energy) are shown in Figure 3b and c, respectively. The intensity profiles of linecuts through the center of the images are displayed in Figure 3d. The fwhm of the confocal image linecut ($P_{donut} = 0$) is 271 ± 2 nm, consistent with the diffraction-limited resolution of our confocal microscope. At $P_{donut} = 32$ mW, near the highest power available in our setup, the fwhm shrinks by a factor of ∼3 to $\Delta d = 89 \pm 2$ nm. At this power, we observe a ∼2-fold reduction in peak fluorescence intensity (see Figure S5), likely because of imperfect donut contrast. We also observe a slight increase in background due, in part, to anti-Stokes fluorescence (Section SVII).

The data in Figure 3a were fit to a commonly used approximation for STED resolution:[34]

$$\Delta d(P_{donut}) \approx \frac{D}{\sqrt{1 + \frac{P_{donut}}{P_{donut,sat}}}} \quad (1)$$

Here D is the confocal microscope resolution, which we set to $D = 270$ nm based on independent measurements, and $P_{donut,sat}$ is a fitted characteristic power that satisfies $\Delta d(P_{donut,sat}) = D/\sqrt{2}$. From the fits (solid red and blue curves), we extract $P_{donut,sat} = 4.8 \pm 0.1$ and 4.7 ± 0.3 mW for two different SiV centers. These powers correspond to characteristic peak pulse fluences of 9.7 ± 0.2 and 9.5 ± 0.6 mJ/cm^2, respectively (Section SV).

The theoretical resolution for a perfect donut beam focused with an $NA_{ideal} = 1.3$ objective (solid black line in Figure 3a) is approximated from a numerical model (Section SV) incorporating the previously measured $\sigma_{STED} = 4 \times 10^{-17}$ cm^2. The corresponding saturation power for this ideal case is $P_{donut,sat} = 2.3$ mW, approximately 2 times smaller than the observed value. Experimentally, we measure a donut beam profile that is more consistent with an effective numerical aperture of $NA_{eff} = 1.1$. This may be due to wavefront or polarization distortions of the STED beam and/or under-filling of the beam at the objective's back aperture (see Section SV). On incorporating this NA into the numerical model (dashed black line in Figure 3a), we find excellent agreement with the

DOI: 10.1021/acsphotonics.9b01135
ACS Photonics 2019, 6, 2577−2582

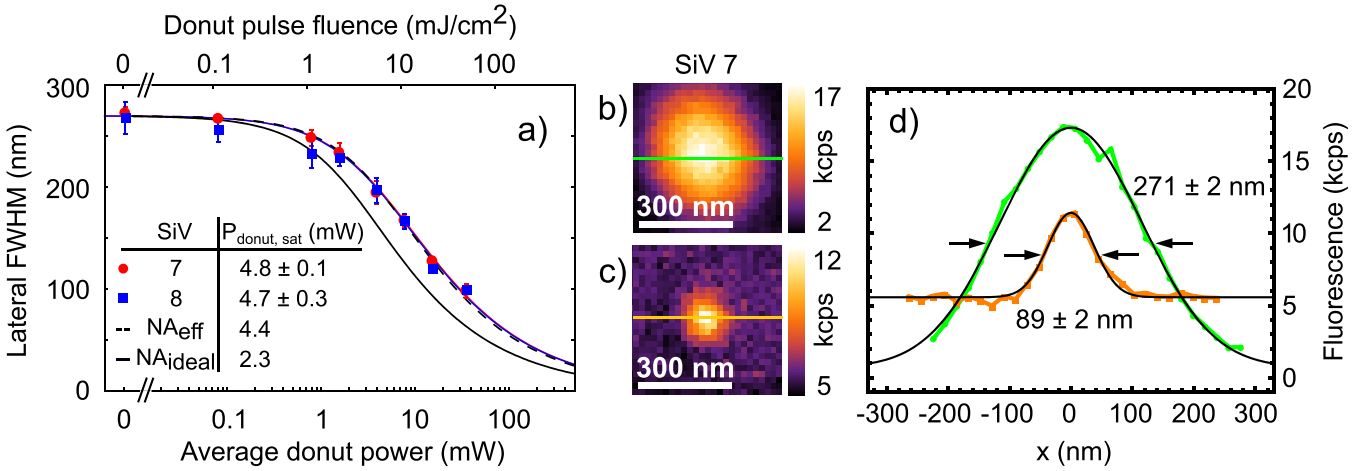

Figure 3. STED resolution enhancement. (a) Lateral fwhm of STED profiles of two isolated SiV centers as a function of average donut power (or corresponding peak pulse fluence). Solid red and blue lines are fits to eq 1 with fitted average donut saturation powers given in the inset. Solid and dashed black lines are the theoretical resolution (Section SV) for an ideal donut profile (NA_{ideal} = 1.3) and the experimentally measured donut profile (NA_{eff} = 1.1), respectively. A lateral fwhm of ∼20 nm is expected at P_{donut} = 400 mW, which corresponds to a pulse energy (5 nJ) commonly used in STED microscopy.[33] (b) Confocal and (c) STED image of an isolated SiV center taken at P_{donut} = 32 mW (0.4 nJ pulse energy). Annotated linecuts are plotted in (d). The fwhm of the confocal profile (green) is reduced by a factor of 3 when applying the STED donut beam (orange). Black curves in (d) are Gaussian fits, and annotated values are their fitted fwhm.

experimental resolution. The corresponding saturation power, $P_{donut,sat}$ = 4.4 mW, is consistent with the fits to eq 1.

Finally, we used STED microscopy to resolve SiV centers spaced closer than the optical diffraction limit. Figure 4 compares confocal and STED images of SiV clusters in two different high-SiV-density regions (Section SII). Unlike the confocal images (Figure 4a,b), the STED images (Figure 4c,d) clearly resolve SiV centers separated by ≲150 nm. Taking into account the similar brightness and fwhm of features in the STED images (see Section SVI), it is likely that each individual SiV center in the scan region is resolved. Figure 4e shows linecuts through a subregion containing closely spaced SiV centers (dashed lines in Figure 4b,d). While the confocal image contains little information about the SiV locations, Gaussian fits to the STED linecut reveal two SiV centers separated by 154 ± 2 nm.

DISCUSSION AND CONCLUSION

The demonstration of super-resolution STED microscopy with SiV centers has implications for several applications. Importantly, all SiV centers studied here showed perfect photostability (no blinking or bleaching), even under continuous illumination with high STED intensity for several days. However, future work is needed to validate the utility of SiV STED microscopy in biological samples. The modest resolution realized here (∼90 nm) was limited by the maximum STED pulse energy (∼0.4 nJ) available in our setup. If a realistic pulse energy of 5 nJ was used, the resolution would improve to $\Delta d \approx 20$ nm for an optimized STED beam profile (Figure 3a). This compares favorably to the STED resolution realized with organic dye molecules ($\Delta d \approx 35$ nm) under similar conditions.[33,35]

Widespread adoption of SiV probes in STED microscopy will also require development of high-yield methods for fabricating monodisperse sub-10 nm SiV-doped nanodiamonds.[36] If SiV centers in these nanodiamonds have similar photophysical properties to those in bulk diamond, as suggested in prior work,[26,37,38] they may be ideal probes for super-resolution biological imaging. SiV STED microscopy

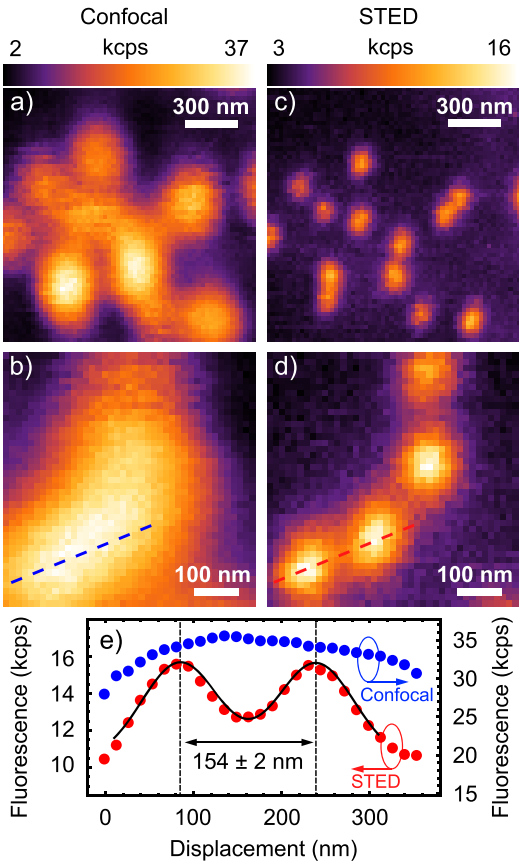

Figure 4. Resolving SiV clusters in diamond. (a, b) Confocal and (c, d) corresponding STED images (P_{donut} = 32 mW) of SiV clusters in two different high-SiV-density regions. The pixel dwell time was 0.1 s. For (a) and (c) the total image acquisition time was 6 min, and for (b) and (d) it was 3 min. (e) Linecuts of the confocal (blue) and STED (red) images across the dashed lines annotated in (b) and (d), respectively. The black solid line is a fit to two Gaussian functions, revealing a SiV center separation of 154 ± 2 nm.

DOI: 10.1021/acsphotonics.9b01135
ACS Photonics 2019, 6, 2577−2582

may also be adapted for super-resolution thermal imaging[39,40] or multiphoton microscopy.[38] In addition, our microscope is well suited for the study of nanoscale arrays of SiV centers for applications in quantum information.[30,31]

In summary, we demonstrated that SiV centers can be used as photostable fluorophores in STED microscopy. We determined the SiV stimulated-emission cross section for 765−800 nm light to be $\sigma_{STED} = (4.0 \pm 0.3) \times 10^{-17}$ cm^2, a factor of 2−4 larger than that of NV centers and approaching that of common organic dye molecules. Our results hold promise for future applications in biological imaging and quantum information.

■ ASSOCIATED CONTENT

Supporting Information

The Supporting Information is available free of charge on the ACS Publications website at DOI: 10.1021/acsphotonics.9b01135.

Microscope setup, sample preparation, pulse fluence and cross section calculations, temporal characterization of laser pulses, lateral point-spread function in STED microscopy, fluorescence intensity distribution of isolated SiV centers, and anti-Stokes excitation (PDF)

■ AUTHOR INFORMATION

Corresponding Author

*E-mail: vmacosta@unm.edu.

ORCID

Victor M. Acosta: 0000-0003-0058-9954

Author Contributions

All authors contributed to the conception and design of the experiment, collection, and analysis of the data and writing of the manuscript.

Author Contributions

§Y. Silani and F. Hubert contributed equally to this work.

Notes

The authors declare no competing financial interest.

■ ACKNOWLEDGMENTS

This work was supported by a Beckman Young Investigator Award and National Science Foundation grant (DMR 1809800). We gratefully acknowledge advice and support from A. Laraoui, I. Fescenko, J.-C. Diels, A. Rastegari, N. Mosavian, J. Damron, N. Ristoff, M. D. Aiello, P. Kehayias, A. Jarmola, A. S. Backer, P. R. Hemmer, K. A. Lidke, and C. Oncebay. We acknowledge the use of nanofabrication and characterization resources at the Department of Energy Center for Integrated Nanotechnologies (CINT).

■ REFERENCES

(1) Hell, S. W.; Wichmann, J. Breaking the diffraction resolution limit by stimulated emission: stimulated-emission-depletion fluorescence microscopy. *Opt. Lett.* **1994**, *19*, 780.

(2) Klar, T. A.; Hell, S. W. Subdiffraction resolution in far-field fluorescence microscopy. *Opt. Lett.* **1999**, *24*, 954.

(3) Westphal, V.; Hell, S. W. Nanoscale resolution in the focal plane of an optical microscope. *Phys. Rev. Lett.* **2005**, *94*, 143903.

(4) Hell, S. W. Toward fluorescence nanoscopy. *Nat. Biotechnol.* **2003**, *21*, 1347.

(5) Pawley, J. *Handbook of Biological Confocal Microscopy*, 3rd ed.; Springer US, 2006; pp 338−342.

(6) Wurm, C. A.; Kolmakov, K.; Göttfert, F.; Ta, H.; Bossi, M.; Schill, H.; Berning, S.; Jakobs, S.; Donnert, G.; Belov, V. N.; Hell, S. W. Novel red fluorophores with superior performance in STED microscopy. *Optical Nanoscopy* **2012**, *1*, 7.

(7) Sameiro, M.; Gonçalves, T. Fluorescent labeling of biomolecules with organic probes. *Chem. Rev.* **2009**, *109*, 190−212.

(8) Choyke, P. L.; Alford, R.; Simpson, H. M.; Duberman, J.; Craig Hill, G.; Ogawa, M.; Regino, C.; Kobayashi, H. Toxicity of organic fluorophores used in molecular imaging: Literature review. *Molecular Imaging* **2009**, *8*, 341−354.

(9) Dempsey, G. T.; Vaughan, J. C.; Chen, K. H.; Bates, M.; Zhuang, X. Evaluation of fluorophores for optimal performance in localization-based super-resolution imaging. *Nat. Methods* **2011**, *8*, 1027−1036.

(10) Bouzin, M.; Chirico, G.; D'Alfonso, L.; Sironi, L.; Soavi, G.; Cerullo, G.; Campanini, B.; Collini, M. Stimulated emission properties of fluorophores by CW-STED single molecule spectroscopy. *J. Phys. Chem. B* **2013**, *117*, 16405−16415.

(11) Donnert, G.; Keller, J.; Medda, R.; Andrei, M. A.; Rizzoli, S. O.; Luhrmann, R.; Jahn, R.; Eggeling, C.; Hell, S. W. Macromolecular-scale resolution in biological fluorescence microscopy. *Proc. Natl. Acad. Sci. U. S. A.* **2006**, *103*, 11440−11445.

(12) Eggeling, C.; Widengren, J.; Rigler, R.; Seidel, C. A. M. Photobleaching of Fluorescent Dyes under Conditions Used for Single-Molecule Detection: Evidence of Two-Step Photolysis. *Anal. Chem.* **1998**, *70*, 2651.

(13) Oracz, J.; Westphal, V.; Radzewicz, C.; Sahl, S. J.; Hell, S. W. Photobleaching in STED nanoscopy and its dependence on the photon flux applied for reversible silencing of the fluorophore. *Sci. Rep.* **2017**, *7*, 11354.

(14) Aharonovich, I.; Neu, E. Diamond nanophotonics. *Adv. Opt. Mater.* **2014**, *2*, 911−928.

(15) Tisler, J.; Balasubramanian, G.; Naydenov, B.; Kolesov, R.; Grotz, B.; Reuter, R.; Boudou, J. P.; Curmi, P. A.; Sennour, M.; Thorel, A.; Börsch, M.; Aulenbacher, K.; Erdmann, R.; Hemmer, P. R.; Jelezko, F.; Wrachtrup, J. Fluorescence and spin properties of defects in single digit nanodiamonds. *ACS Nano* **2009**, *3*, 1959−1965.

(16) Man, H. B.; Ho, D. Nanodiamonds as platforms for biology and medicine. *Journal of Laboratory Automation* **2013**, *18*, 12−18.

(17) Wildanger, D.; Patton, B. R.; Schill, H.; Marseglia, L.; Hadden, J. P.; Knauer, S.; Schönle, A.; Rarity, J. G.; O'Brien, J. L.; Hell, S. W.; Smith, J. M. Solid immersion facilitates fluorescence microscopy with nanometer resolution and sub-Ångström emitter localization. *Adv. Mater.* **2012**, *24*, 309−313.

(18) Faklaris, O.; Botsoa, J.; Sauvage, T.; Roch, J. F.; Treussart, F. Photoluminescent nanodiamonds: Comparison of the photoluminescence saturation properties of the NV color center and a cyanine dye at the single emitter level, and study of the color center concentration under different preparation conditions. *Diamond Relat. Mater.* **2010**, *19*, 988−995.

(19) Han, K. Y.; Willig, K. I.; Rittweger, E.; Jelezko, F.; Eggeling, C.; Hell, S. W. Three-dimensional stimulated emission depletion microscopy of nitrogen-vacancy centers in diamond using continuous-wave light. *Nano Lett.* **2009**, *9*, 3323−3329.

(20) Rittweger, E.; Han, K. Y.; Irvine, S. E.; Eggeling, C.; Hell, S. W. STED microscopy reveals crystal colour centres with nanometric resolution. *Nat. Photonics* **2009**, *3*, 144−147.

(21) Aslam, N.; Waldherr, G.; Neumann, P.; Jelezko, F.; Wrachtrup, J. Photo-induced ionization dynamics of the nitrogen vacancy defect in diamond investigated by single-shot charge state detection. *New J. Phys.* **2013**, *15*, 013064.

(22) Hacquebard, L.; Childress, L. Charge-state dynamics during excitation and depletion of the nitrogen-vacancy center in diamond. *Phys. Rev. A: At., Mol., Opt. Phys.* **2018**, *97*, 063408.

(23) Rabeau, J. R.; Stacey, A.; Rabeau, A.; Prawer, S.; Jelezko, F.; Mirza, I.; Wrachtrup, J. Single nitrogen vacancy centers in chemical vapor deposited diamond nanocrystals. *Nano Lett.* **2007**, *7*, 3433−3437.

(24) Hepp, C.; Müller, T.; Waselowski, V.; Becker, J. N.; Pingault, B.; Sternschulte, H.; Steinmüller-Nethl, D.; Gali, A.; Maze, J. R.;

DOI: 10.1021/acsphotonics.9b01135
ACS Photonics 2019, 6, 2577−2582

Atatüre, M.; Becher, C. Electronic structure of the silicon vacancy color center in diamond. *Phys. Rev. Lett.* **2014**, *2*, 036405.
(25) Rogers, L. J.; Jahnke, K. D.; Doherty, M. W.; Dietrich, A.; McGuinness, L. P.; Müller, C.; Teraji, T.; Sumiya, H.; Isoya, J.; Manson, N. B.; Jelezko, F. Electronic structure of the negatively charged silicon-vacancy center in diamond. *Phys. Rev. B: Condens. Matter Mater. Phys.* **2014**, *89*, 235101.
(26) Vlasov, I.; Shiryaev, A. A.; Rendler, T.; Steinert, S.; Lee, S. Y.; Antonov, D.; Vörös, M.; Jelezko, F.; Fisenko, A. V.; Semjonova, L. F.; Biskupek, J.; Kaiser, U.; Lebedev, O. I.; Sildos, I.; Hemmer, P. R.; Konov, V. I.; Gali, A.; Wrachtrup, J. Molecular-sized fluorescent nanodiamonds. *Nat. Nanotechnol.* **2014**, *9*, 54−58.
(27) Wang, C.; Kurtsiefer, C.; Weinfurter, H.; Burchard, B. Single photon emission from SiV centres in diamond produced by ion implantation. *J. Phys. B: At., Mol. Opt. Phys.* **2006**, *39*, 37−41.
(28) Kastrup, L.; Hell, S. W. Absolute optical cross section of individual fluorescent molecules. *Angew. Chem., Int. Ed.* **2004**, *43*, 6646.
(29) Rittweger, E.; Rankin, B. R.; Westphal, V.; Hell, S. W. Fluorescence depletion mechanisms in super-resolving STED microscopy. *Chem. Phys. Lett.* **2007**, *442*, 483−487.
(30) Tamura, S.; Koike, G.; Komatsubara, A.; Teraji, T.; Onoda, S.; McGuinness, L. P.; Rogers, L.; Naydenov, B.; Wu, E.; Yan, L.; Jelezko, F.; Ohshima, T.; Isoya, J.; Shinada, T.; Tanii, T. Array of bright silicon-vacancy centers in diamond fabricated by low-energy focused ion beam implantation. *Appl. Phys. Express* **2014**, *7*, 115201.
(31) Schröder, T.; Trusheim, M. E.; Walsh, M.; Li, L.; Zheng, J.; Schukraft, M.; Sipahigil, A.; Evans, R. E.; Sukachev, D. D.; Nguyen, C. T.; Pacheco, J. L.; Camacho, R. M.; Bielejec, E. S.; Lukin, M. D.; Englund, D. Scalable focused ion beam creation of nearly lifetime-limited single quantum emitters in diamond nanostructures. *Nat. Commun.* **2017**, *8*, 15376.
(32) Gregor, I.; Patra, D.; Enderlein, J. Optical saturation in fluorescence correlation spectroscopy under continuous-wave and pulsed excitation. *ChemPhysChem* **2005**, *6*, 164.
(33) Wildanger, D.; Medda, R.; Kastrup, L.; Hell, S. W. A compact STED microscope providing 3D nanoscale resolution. *J. Microsc.* **2009**, *236*, 35−43.
(34) Harke, B.; Keller, J.; Ullal, C. K.; Westphal, V.; Schoenle, A.; Hell, S. W. Resolution scaling in STED microscopy. *Opt. Express* **2008**, *16*, 4154−4162.
(35) Wildanger, D.; Rittweger, E.; Kastrup, L.; Hell, S. W. STED microscopy with a supercontinuum laser source. *Opt. Express* **2008**, *16*, 9614−21.
(36) Crane, M. J.; Petrone, A.; Beck, R. A.; Lim, M. B.; Zhou, X.; Li, X.; Stroud, R. M.; Pauzauskie, P. J. High-pressure, high-temperature molecular doping of nanodiamond. *Science Advances* **2019**, *5*, No. eaau6073.
(37) Neu, E.; Steinmetz, D.; Riedrich-Möller, J.; Gsell, S.; Fischer, M.; Schreck, M.; Becher, C. Single photon emission from silicon-vacancy colour centres in chemical vapour deposition nano-diamonds on iridium. *New J. Phys.* **2011**, *13*, 025012.
(38) Higbie, J. M.; Perreault, J. D.; Acosta, V. M.; Belthangady, C.; Lebel, P.; Kim, M. H.; Nguyen, K.; Demas, V.; Bajaj, V.; Santori, C. Multiphoton-Excited Fluorescence of Silicon-Vacancy Color Centers in Diamond. *Phys. Rev. Appl.* **2017**, *7*, 054010.
(39) Neu, E.; Hepp, C.; Hauschild, M.; Gsell, S.; Fischer, M.; Sternschulte, H.; Steinmüller-Nethl, D.; Schreck, M.; Becher, C. Low-temperature investigations of single silicon vacancy colour centres in diamond. *New J. Phys.* **2013**, *15*, 043005.
(40) Nguyen, C. T.; Evans, R. E.; Sipahigil, A.; Bhaskar, M. K.; Sukachev, D. D.; Agafonov, V. N.; Davydov, V. A.; Kulikova, L. F.; Jelezko, F.; Lukin, M. D. All-optical nanoscale thermometry with silicon-vacancy centers in diamond. *Appl. Phys. Lett.* **2018**, *7*, 054010.

DOI: 10.1021/acsphotonics.9b01135
ACS Photonics 2019, 6, 2577−2582